

Capture of CO₂ during the Electrolysis Process and Its Utilization in Supercapacitor Materials

Published as part of ACS Omega virtual special issue "CO₂ Geostorage".

Mengjun Hu, Rui Tan,* Xiaojuan Jiang, Mengyao Dong, Liangying Wen, and Meilong Hu*



Cite This: *ACS Omega* 2024, 9, 6888–6893



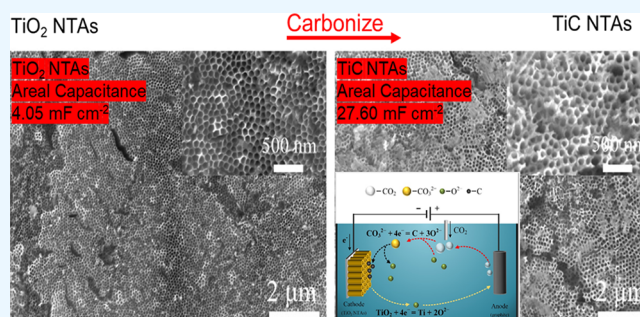
Read Online

ACCESS |

Metrics & More

Article Recommendations

ABSTRACT: With climate change and environmental issues, the emissions of CO₂ and its greenhouse effect have become a focal point. At present, the utilization of CO₂ includes its synthesis into chemicals and fuels such as methane, methanol, and CO. CO₂ utilization can be achieved through carbon capture and storage technologies, which involve capturing CO₂ from industrial emissions and storing it to reduce the CO₂ concentration in the atmosphere. However, these CO₂ capture and utilization technologies still face challenges, such as technical immaturity and high costs. One of the CO₂ capture and utilization technologies is the production of energy storage materials. In this study, CO₂ captured by molten salt was used as the carbon source, and TiO₂ nanotube arrays were used as precursors. Titanium carbide nanotube arrays (TiC-NTAs) with high specific surface area and high conductivity were prepared by electrolysis. Afterward, the electrochemical energy storage performance of TiC in different electrolytes was tested. The results show that reducing the ionic radius of the electrolyte is conducive to increasing the area-specific capacitance of the device and that the degradation of the cycle life of the quasi-solid supercapacitor may be caused by an increase in the internal resistance due to the loss of water from the electrolyte. This study provides a reference value for the low-temperature synthesis of nanometal carbides and the selection of electrolytes.



1. INTRODUCTION

The research found that the use of carbon anodes in the molten salt electrolysis process leads to contamination of both electrolytic products and molten salt and reduces the electrolytic efficiency of the process. There are many types of research related to the effects of carbon on the electrochemical process,^{1–8} as shown in Table 1. The results show that when carbon is used as an anode to prepare a metal, the final product and molten salt would be carbon contaminated, such as TiC, Cr₇C₃, VC, and so on. Based on this condition, there are many researches to use these carbon resources.^{1–3} The results show that carbon and oxygen can be obtained by the capture of CO₂ in the molten salt. Here, we conducted a preliminary study on the utilization of carbon sources resulting from the use of carbon anodes, primarily for the reduction of TiO₂ nanotube arrays (TiO₂ NTAs) into highly conductive and capacitance-enhanced TiC nanotube arrays (TiC NTAs).⁹ The research results indicate that CO₃²⁻ formed by carbon dioxide dissolved in molten salt generated by the carbon anode during electrolysis, in combination with carbon produced through cathodic electrochemical carbon deposition and metallic titanium from cathodic TiO₂ electrolytic deoxygenation, can react to form TiC. By adjusting the composition of

the molten salt, enhance wetting between the molten salt and TiO₂ nanotubes can be achieved, enabling the molten salt to enter the nanotubes and achieving overall carbonization of TiO₂ nanotube arrays into TiC NTAs. This research proposes using this process to capture carbon dioxide for the preparation of capacitor materials. It explores suitable electrolyte systems for the efficient operation of TiC nanotube arrays as supercapacitor electrode materials. In the face of increasingly severe environmental and energy issues, this research contributes to reducing carbon dioxide emissions.

2. EXPERIMENTAL SECTION

2.1. Preparation of TiC NTAs. The process of capturing and converting carbon dioxide as a carbon source to synthesize TiC NTAs has been described in a published paper.¹² During

Received: October 21, 2023

Revised: December 29, 2023

Accepted: January 5, 2024

Published: February 4, 2024



Table 1. Literature about Carbon Contamination during Molten Salt Electrolysis

topic	effects of carbon	references
direct electrochemical production of Ti-10W alloys from the mixed oxides	the surface of the sample is carbon-rich and TiC is detected	Dring et al. ⁴
electrochemical reduction mechanism of Nb ₂ O ₅	there is NbC on the product surface	Vishnu et al. ⁵
the influence of graphite anode and SnO ₂ -based inert anode on the current efficiency of Cr ₂ O ₃ deoxidation	there is obvious carbon contamination in molten salt, and Cr ₇ C ₃ appears in chromium products	Kilby et al. ⁶
electrochemical reduction of K ₂ CrO ₄ in molten salt using liquid zinc cathode	liquid zinc cathode avoids product contamination, but there is still molten salt contamination	Weng et al. ⁷
preparation of metal Ti in CaCl ₂ -based melt	carbon powder is floating on the surface of molten salt and TiC in the titanium product is detected.	Suzuki et al. ⁸
electrolytic reduction of V ₃ S ₄ in molten CaCl ₂	there is obvious molten salt contamination when electrolyzing V ₂ O ₃	Matsuzaki et al. ⁹
one-step electrochemical preparation of metallic vanadium from sodium metavanadate in molten chlorides	carbon contamination exists in molten salt and VC is mixed in vanadium products	Weng et al. ¹⁰
electrodeoxidation of porous TiO ₂ in molten calcium chloride	there is a large amount of carbon powder near the cathode and on the surface of the melt	Schwandt et al. ¹¹

the electrolysis process, 0.1 mol % Li₂O is first added to the molten salt to improve its ability to capture carbon dioxide. Then, excess carbon dioxide gas (300 mL) is slowly introduced into the molten salt to ensure that Li₂O is completely converted into Li₂CO₃ (Li₂O + CO₂ = Li₂CO₃). The generated CO₃²⁻ can be reduced to carbon deposited at the cathode. Afterward, TiO₂ electro-deoxidizes and reacts with the deposited carbon to form TiC. Based on formula 1, the calculated decomposition voltages at 600 °C for CaCl₂, KCl, and LiCl are 3.44, 3.49, and 3.66 V, respectively. In this study, the electrolysis voltage was set at 3.3 V.

$$E^{\circ} = -\frac{\Delta_r G_m^{\theta}}{nF} \quad (1)$$

In the equation, E represents the theoretical decomposition voltage (V), $\Delta_r G_m^{\theta}$ represents the standard Gibbs free energy change of the electrode reaction (J/mol), n represents the number of electrons involved in the reaction equation, and F represents the Faraday constant (96485 C/mol).

2.2. Preparation of an Electrolyte. Preparation of the PVA–Na₂SO₄ gel electrolyte. Under the condition of magnetic stirring at 80 °C, 6 g PVA was slowly added to 60 mL deionized water and stirred continuously for 1 h until PVA was completely dissolved. After that, 20 mL of 1 mol/L Na₂SO₄ solution was added to the PVA solution, and the solution was continuously stirred for 30 min and then cooled to room temperature. The prepared solution was poured into the plastic mold, and after that it was spread and leveled. It was physically blended through two cycles of freeze–thaw (placed at 20 and 20 °C for 12 h, respectively).

Preparation of the PVA–KOH gel electrolyte. 6 g PVA was slowly added into 60 mL deionized water, and the PVA was completely dissolved by magnetic stirring at 80 °C for 1 h. After that, 20 mL of 1 mol/L KOH solution was added into the PVA solution, which was continuously stirred for 30 min and then cooled to room temperature. The prepared solution was poured into a plastic mold and dried at room temperature to obtain an electrolyte film.

2.3. Characterization. The prepared TiC NTAs were tested for their electrochemical performance. The quasi-solid-state flexible supercapacitor consists of two identical TiC NTA electrode sheets and an electrolyte film sandwiched in the middle, and the overall capacitor shows a sandwich structure. The electrochemical performance of the TiC NTA electrode was studied using a CHI1140C electrochemical workstation (CH Instruments, China), including cyclic voltammetry (CV),

galvanostatic charge/discharge (GCD), cyclic stability, and electrochemical impedance spectroscopy (EIS) testing.

3. RESULTS AND DISCUSSION

3.1. Formation Mechanism of TiC NTAs. Our published work has proven that during the electrolysis process,¹² as

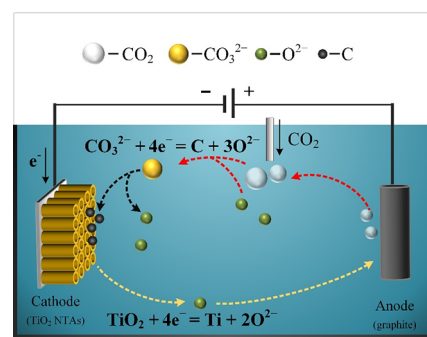


Figure 1. Mechanism diagram of synthesizing TiC NTAs with CO₂ as the carbon source.

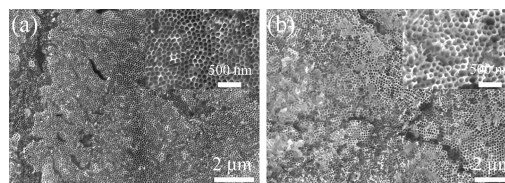


Figure 2. (a) SEM image of TiO₂ NTAs. (b) SEM image of TiC NTAs.

shown in Figure 1, TiO₂ nanotubes first undergo rapid deoxygenation to form titanium's low-valence oxide (eq 2). The conductivity of the precursor rapidly increases. Due to the lower reduction potential of CO₃²⁻ ions compared to that of the low-valence oxide, the carbon dioxide (CO₃²⁻) ion reduction reaction primarily occurs at the cathode. CO₃²⁻ ions near the cathode are reduced on the surface of the nanotubes to form carbon (eq 3). When the concentration of CO₃²⁻ ions near the cathode decreases to a certain level, the deep deoxygenation of titanium's low-valence oxide can take place. However, when the CO₃²⁻ ions in the molten salt further diffuse to the vicinity of the cathode, the deep deoxygenation reaction is suppressed again, and the CO₃²⁻ ions near the cathode are reduced and depleted once more. At this stage, the processes of electrodeoxygenation and carbon

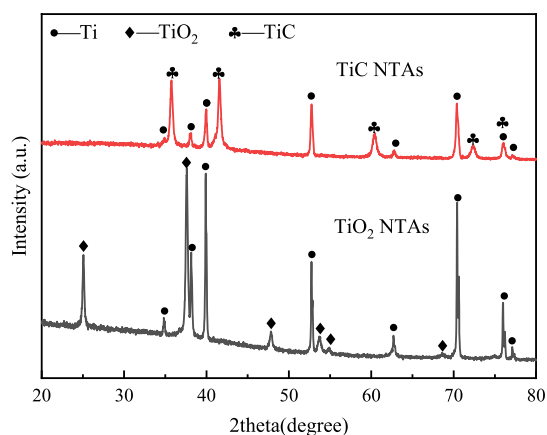
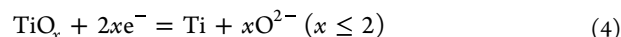
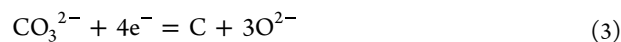
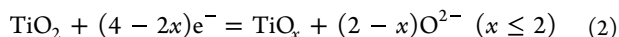


Figure 3. XRD pattern of TiC NTAs and TiO₂ NTAs.

deposition may alternate, and the diffusion of CO₃²⁻ ions toward the cathode becomes a limiting factor for the carbon deposition reaction. When the low-valence oxide of titanium is reduced to metallic Ti (eq 4), the deposited carbon quickly reacts with Ti to form TiC (eq 5).



3.2. Fabrication and Characterization of TiC NTAs.

The capture efficiency of carbon dioxide during the preparation of TiC NTAs is closely related to several conditions. The optimal process includes the following: anodic oxidation time of TiO₂ NTA precursor is 1 h, the electrolysis temperature is 600 °C, the solubility of carbon dioxide or the concentration of CO₃²⁻ ion in molten salt is 0.1 mol %, and the electrolysis time is 1.5 h. From Figure 2a, it can be observed that the TiO₂ NTAs obtained by anodizing are vertically arranged to form an array structure, with a pipe diameter between 90 and 100 nm. Afterward, TiO₂ NTAs were used as cathode precursors and nanostructure templates to obtain TiC NTAs through electrolysis (Figure 2b). From Figure 2b, it can be seen that TiC NTAs still maintain the array structure of TiO₂ nanotubes, and the tube structure remains intact.

Figure 3 shows the XRD patterns of TiO₂ and TiC NTAs. From the figure, it can be seen that after annealing treatment the TiO₂ NTAs are transformed into the anatase phase, and

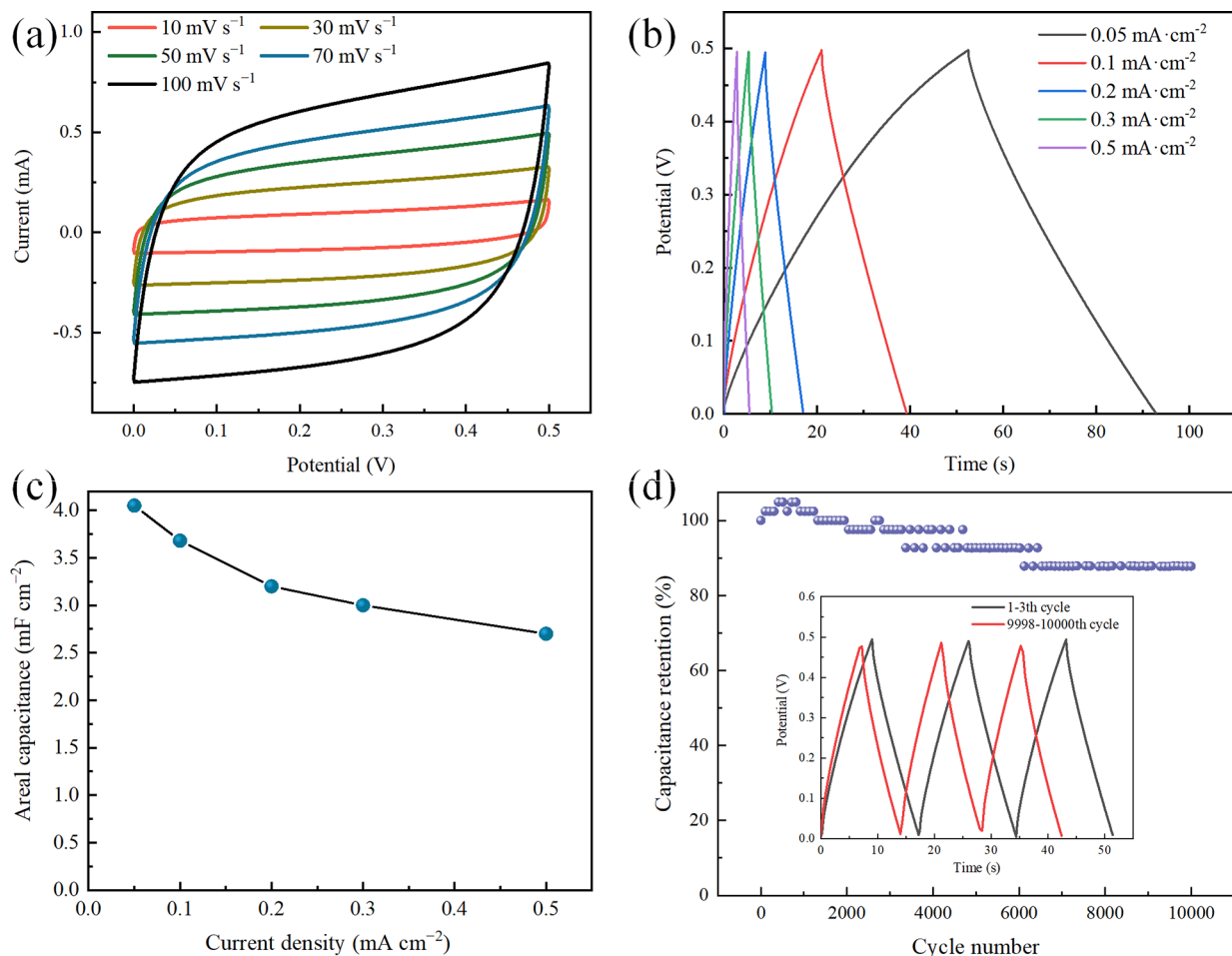


Figure 4. Electrochemical energy storage performance of TiC NTAs electrodes with PVA–Na₂SO₄ as the electrolyte. (a) CV curves at scan rates ranging from 10 to 100 mV s⁻¹; (b) GCD curves at current densities ranging from 0.05 to 0.5 mA cm⁻²; (c) specific capacitances at various current densities; (d) capacitance retention of TiC NTAs for 10,000 cycles at a current density of 0.2 mA cm⁻². Insets are GCD curves for 1–3 cycles and 4998–5000 cycles.

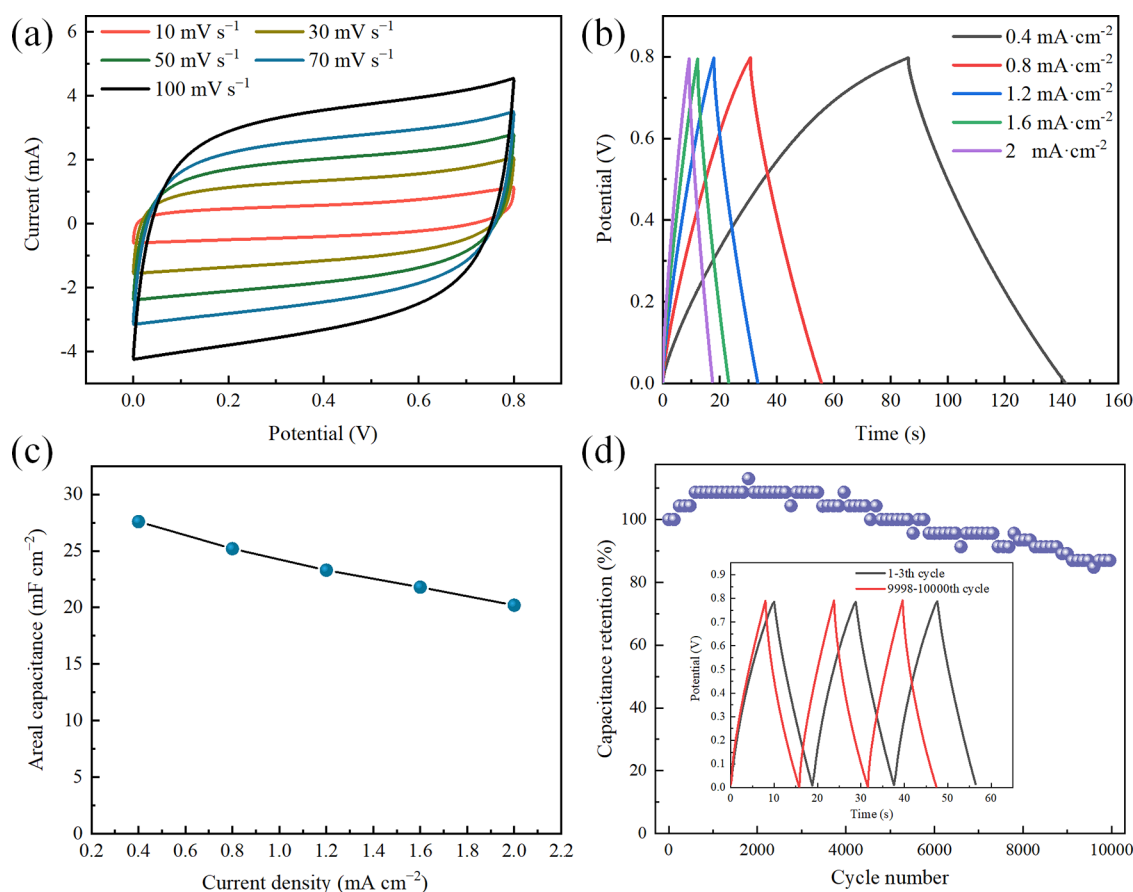


Figure 5. Electrochemical energy storage performance of TiC NTAs electrodes with PVA–KOH as the electrolyte. (a) CV curves at scan rates ranging from 10 to 100 mV s⁻¹; (b) GCD curves at current densities ranging from 0.4 to 2 mA cm⁻²; (c) specific capacitances at various current densities; (d) capacitance retention of TiC NTAs for 10,000 cycles at a current density of 2 mA cm⁻². Insets are GCD curves for 1–3 cycles and 4998–5000 cycles.

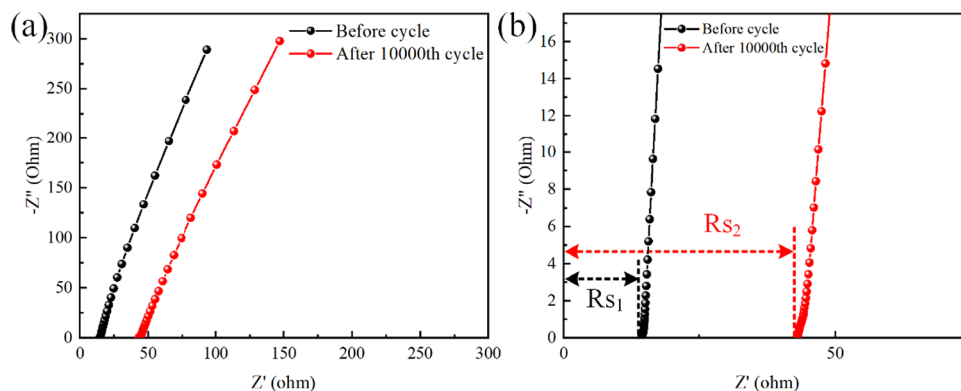


Figure 6. (a) Nyquist plot before and after 10,000 cycles of supercapacitors; (b) enlarged view of the high-frequency region.

the diffraction peaks of titanium mainly come from the titanium substrate. After electrolysis, all the diffraction peaks of TiO₂ disappeared and were replaced by the appearance of diffraction peaks of TiC phase, indicating that TiO₂ deoxidized and carbonized to form TiC.

3.3. Supercapacitor Performance of TiC NTAs.

3.3.1. Electrolyte of PVA–Na₂SO₄. The prepared TiC NTAs were tested for their electrochemical energy storage performance. Figure 4 presents the electrochemical performance test results of the assembled quasi-solid-state supercapacitor using TiC NTAs as both the cathode and the anode, with PVA–Na₂SO₄ polymer as the electrolyte and separator. Figure 4a

shows the cyclic voltammetry curves of the TiC NTA electrode at scan rates of 10–100 mV/s, indicating a nearly rectangular shape at different scan rates and demonstrating the double-layer energy storage characteristics of TiC NTAs. Additionally, the galvanostatic charge–discharge (GCD) curves exhibit good triangular symmetry without apparent shoulder peaks, further confirming the double-layer energy storage behavior. Figure 4c displays the specific area capacitance of the capacitors at various current densities. The specific area capacitance of the capacitor reaches 4.05 mF/cm² at a current density of 0.05 mA/cm², corresponding to a specific area capacitance of 16.2 mF/cm² for an individual electrode, which

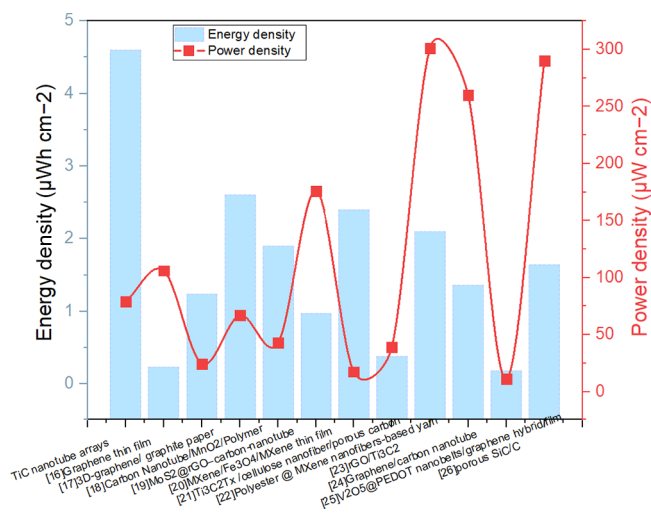


Figure 7. Energy and power densities of different electrode materials.

is lower than the capacitance measured in the Na_2SO_4 solution. This is because the contact area between the $\text{PVA-Na}_2\text{SO}_4$ electrolyte and the electrode material is limited and insufficient contact hinders the effective utilization of some nanostructures, resulting in reduced capacitance. In the Na_2SO_4 solution, the electrolyte can fully infiltrate the nanostructures of the electrode material, enlarging the contact interface between the electrolyte and the electrode, thereby increasing the area for ion adsorption and obtaining a higher capacitance. Figure 3d shows the capacitance retention after 10,000 cycles of TiC NTAs. After 5000 charge–discharge cycles, the capacitance remains at 93% of the initial capacitance, which is higher than that observed with 1 M EMIMBF₄ as the electrolyte. The quasi-solid-state electrolyte can effectively suppress harmful electrochemical oxidation, prevent electrolyte flushing of the electrode, reduce the detachment and pulverization of nanostructures during long-term cycling processes,^{10–12} and thus improve the stability of the TiC NTAs electrode. After 10,000 cycles, the capacitance still retains 88% of the initial capacitance, and the GCD curves maintain charge–discharge symmetry, indicating good cycle stability of TiC NTAs in the quasi-solid-state electrolyte.

3.3.2. Electrolyte of PVA–KOH. Figure 5 illustrates the electrochemical energy storage performance of TiC NTAs in a PVA–KOH gel polymer electrolyte. From the CV and GCD curves, it can be observed that the TiC NTAs electrode maintains typical double-layer energy storage characteristics (Figure 5a,b). Figure 5c displays the specific area capacitance of the capacitors at various current densities. At a current density of 0.4 mA/cm², the specific area capacitance of the capacitor reaches 27.6 mF/cm², which is significantly higher than the capacitance observed with PVA– Na_2SO_4 as the electrolyte. The difference in capacitance between different gel electrolytes is mainly attributed to the ionic radius effect.¹³ OH[−] ions have a smaller ionic radius, facilitating migration into the interior of the nanostructures. As a result, TiC NTAs exhibit a higher capacitance in the PVA–KOH electrolyte. Figure 5d²² shows the capacitance retention after 10,000 cycles of TiC NTAs. It can be observed that during the initial 1000 cycles, the specific area capacitance gradually increases to 109% of the initial value mainly due to the initial self-activation process. In the early cycles, the electrolyte and electrode material gradually come into full contact, and with ion

adsorption/desorption, the number of active sites within the material increases slightly, resulting in a slight increase in capacitance.^{14,15} After 3000 cycles, the capacitance exhibits a stepwise decrease, reaching 87% of the initial value after 10,000 cycles, which is consistent with the cycle life of TiC NTAs in the PVA– Na_2SO_4 electrolyte.

Figure 6 presents a comparison of the AC impedance spectra of the supercapacitor before and after cycling. In Figure 6b, the intercept of the high-frequency region curve on the real axis (Z' axis) corresponds to the internal resistance (R_s), and it can be observed that the internal resistance increases from 14.2 to 42.8 Ω after 10,000 cycles. Additionally, in the high-frequency region, nearly semicircular impedance curves are observed, indicating a small radius of the impedance arc and a low interfacial charge transfer resistance between the electrolyte and electrode material. In the low-frequency region, the slope of the straight line reflects the diffusion extent of electrolyte ions within the electrode. A steeper slope indicates faster ion diffusion during the charge and discharge processes. From Figure 6, it can be seen that the straight lines in the low-frequency region before and after cycling are almost parallel with similar slopes. According to the impedance analysis, it can be concluded that the internal resistance of the electrolyte significantly increases after cycling, indicating a decrease in the conductivity of the polymer, possibly due to dehydration of the gel polymer electrolyte. Therefore, during long-term cycling charge and discharge processes, continuous dehydration of the electrolyte leads to an increase in internal resistance, resulting in capacitance decay.

3.3.3. Electrolyte of PVA– H_3PO_4 . In this section, the PVA– H_3PO_4 gel polymer electrolyte is used to further investigate the influence of electrolyte composition on the performance of TiC NTAs-based supercapacitors. The results of this section have been shown in the published work.¹² When the current density is 0.2 mA cm^{−2} the specific capacitance is 53.3 mF cm^{−2}. The results indicate that the specific capacitance of the TiC NTA electrode in the PVA– H_3PO_4 electrolyte is significantly higher than that in PVA– Na_2SO_4 and PVA–KOH electrolytes. Figure 7 displays the compared energy density and power density between our work and the references. TiC NTAs show excellent energy densities in the PVA– H_3PO_4 electrolyte.^{16–26}

4. CONCLUSIONS

Based on the idea of capturing carbon dioxide during the molten salt electrolysis of metal oxides, this study proposes the utilization of captured carbon dioxide to achieve the carbonization of TiO_2 NTAs into TiC NTAs through electrochemical deoxygenation. In addition, TiC NTAs were used as electrode materials in supercapacitors, and their electrochemical energy storage performance in different electrolytes was compared. The results indicate that reducing the ion radius of the electrolyte is beneficial for improving the area-specific capacitance of the device. When the electrolyte changes from Na_2SO_4 to KOH, the area-specific capacitance of the device increases from 4.05 to 27.6 mF cm^{−2}. After 10,000 cycles of charging and discharging, the retained capacitance values are 88% (PVA– Na_2SO_4) and 87% (PVA–KOH) of the initial value, respectively. This is due to the increase of internal resistance caused by water loss of the gel polymer electrolyte, which leads to capacitance attenuation. This study provides a reference value for the low-temperature synthesis of nanometal carbides and the selection of electrolytes.

AUTHOR INFORMATION

Corresponding Authors

Rui Tan – School of Materials Science and Engineering, Chongqing University, Chongqing 400044, China; Email: 18269785642@163.com

Meilong Hu – School of Materials Science and Engineering, Chongqing University, Chongqing 400044, China; orcid.org/0000-0002-5071-0700; Email: hml@cqu.edu.cn

Authors

Mengjun Hu – Key Laboratory of Material Processing and Mold Technology, School of Mechanical Engineering and Automation, Chongqing Industry Polytechnic College, Chongqing 401120, China

Xiaojuan Jiang – Key Laboratory of Material Processing and Mold Technology, School of Mechanical Engineering and Automation, Chongqing Industry Polytechnic College, Chongqing 401120, China

Mengyao Dong – Key Laboratory of Material Processing and Mold Technology, School of Mechanical Engineering and Automation, Chongqing Industry Polytechnic College, Chongqing 401120, China

Liangying Wen – School of Materials Science and Engineering, Chongqing University, Chongqing 400044, China

Complete contact information is available at:

<https://pubs.acs.org/10.1021/acsomega.3c07587>

Funding

This work was supported by the Chongqing Natural Science Foundation (cstc2021jcyj-msxmX1049).

Notes

The authors declare no competing financial interest.

REFERENCES

- (1) Yin, H. Y.; Mao, X. H.; Tang, D. Y.; et al. Capture and electrochemical conversion of CO₂ to value-added carbon and oxygen by molten salt electrolysis. *Energy Environ. Sci.* **2013**, *6* (5), 1538–1545.
- (2) Kaplan, V.; Wachtel, E.; Lubomirsky, I. CO₂ to CO Electrochemical Conversion in Molten Li₂CO₃ Is Stable with Respect to Sulfur Contamination. *J. Electrochem. Soc.* **2014**, *161* (1), F54–F57.
- (3) Kaplan, B.; Groult, H.; Barhoun, A.; et al. Synthesis and structural characterization of carbon powder by electrolytic reduction of molten Li₂CO₃-Na₂CO₃-K₂CO₃. *J. Electrochem. Soc.* **2002**, *149* (5), D72–D78.
- (4) Dring, K.; Bhagat, R.; Jackson, M.; et al. Direct electrochemical production of Ti-10W alloys from mixed oxide preform precursors. *J. Alloys Compd.* **2006**, *419* (1–2), 103–109.
- (5) Vishnu, D. Sri Maha; Sanil, N.; Shakila, L.; et al. A study of the reaction pathways during electrochemical reduction of dense Nb₂O₅ pellets in molten CaCl₂ medium. *Electrochim. Acta* **2013**, *100*, 51–62.
- (6) Kilby, K. T.; Jiao, S.; Fray, D. J. Current efficiency studies for graphite and SnO₂-based anodes for the electro-deoxidation of metal oxides. *Electrochim. Acta* **2010**, *55* (23), 7126–7133.
- (7) Weng, W.; Wang, Z.; Guo, Z.; et al. Enhanced electrodeposition and separation of metallic Cr from soluble K₂CrO₄ on a liquid Zn cathode. *J. Energy Chem.* **2020**, *40*, 204–211.
- (8) Suzuki, R. O.; Noguchi, H.; Haraguchi, Y.; et al. Metal Production in CaCl₂-Based Melts. *ECS Trans.* **2018**, *86* (14), 45.
- (9) Matsuzaki, T.; Natsui, S.; Kikuchi, T.; et al. Electrolytic reduction of V₃S₄ in molten CaCl₂. *Mater. Trans.* **2017**, *58* (3), 371–376.
- (10) Weng, W.; Wang, M.; Gong, X.; et al. Mechanism analysis of carbon contamination and the inhibition by an anode structure during soluble K₂CrO₄ electrolysis in CaCl₂-KCl molten salt. *J. Electrochem. Soc.* **2017**, *164* (12), E360–E366.
- (11) Schwandt, C.; Alexander, D. T. L.; Fray, D. J. The electro-deoxidation of porous titanium dioxide precursors in molten calcium chloride under cathodic potential control. *Electrochim. Acta* **2009**, *54* (14), 3819–3829.
- (12) Ma, Tongxiang; Tan, Rui; Chen, Junyu; Pan, Yuzheng; Han, Guang; Liwen, Hu; Yan, Zhiming Low-Temperature Fabrication of TiC Nanotube Arrays by Molten Salt Electrolysis for Supercapacitor Application. *ACS Appl. Energy Mater.* **2022**, *5*, 13843–13850.
- (13) Li, W.; Liu, Q.; Chen, S.; et al. Single-crystalline integrated 4H-SiC nanochannel array electrode: Toward high-performance capacitive energy storage for robust wide-temperature operation. *Materials Horizons* **2018**, *5* (5), 883–889.
- (14) Chen, G. Z.; Fray, D. J. Invention and fundamentals of the FFC Cambridge Process. *Extr. Metall. Titanium* **2019**, 227–286, DOI: 10.1016/B978-0-12-817200-1.00011-9.
- (15) Shivaram, A.; Bose, S.; Bandyopadhyay, A. Thermal degradation of TiO₂ nanotubes on titanium. *Appl. Surf. Sci.* **2014**, *317*, 573–580.
- (16) Chen, Q.; Li, X.; Zang, X.; et al. Effect of different gel electrolytes on graphene-based solid-state supercapacitors. *RSC Adv.* **2014**, *4* (68), 36253–36256.
- (17) Ramadoss, A.; Yoon, K. Y.; Kwak, M. J.; et al. Fully flexible, lightweight, high-performance all-solid-state supercapacitor based on 3-dimensional graphene/graphite paper. *J. Power Sources* **2017**, *337*, 159–165.
- (18) Choi, C.; Kim, S. H.; Sim, H. J.; et al. Stretchable, weavable coiled carbon nanotube/MnO₂/polymer fiber solid-state supercapacitors. *Sci. Rep.* **2015**, *5*, 9387.
- (19) Li, W.; Liu, Q.; Fang, Z.; et al. All-solid-state on-chip supercapacitors based on free-standing 4H-SiC nanowire arrays. *Adv. Energy Mater.* **2019**, *9* (17), No. 1900073.
- (20) Li, H.; Liu, Y.; Lin, S.; et al. Laser-crystallized sandwich-like MXene/Fe₃O₄/MXene thin film electrodes for flexible supercapacitors. *J. Power Sources* **2021**, *497*, No. 229882.
- (21) Chen, W.; Zhang, D.; Yang, K.; et al. Mxene (Ti₃C₂T_x)/cellulose nanofiber/porous carbon film as a free-standing electrode for ultrathin and flexible supercapacitors. *Chem. Eng. J.* **2021**, *413*, No. 127524.
- (22) Shao, W.; Tebyetekerwa, M.; Marriam, I.; et al. Polyester@MXene nanofibers-based yarn electrodes. *J. Power Sources* **2018**, *396*, 683–690.
- (23) Radha, N.; Kanakaraj, A.; Manohar, H. M.; et al. Binder free self-standing high-performance supercapacitor electrode based on graphene/titanium carbide composite aerogel. *Appl. Surf. Sci.* **2019**, *481*, 892–899.
- (24) Wang, Y.; Zhang, Y.; Wang, G.; et al. Direct graphene-carbon nanotube composite ink writing all-solid-state flexible micro-supercapacitors with high areal energy density. *Adv. Funct. Mater.* **2020**, *30* (16), No. 1907284.
- (25) Wang, L.; Shu, T.; Guo, S.; et al. Fabricating strongly coupled V₂O₅@PEDOT nanobelts/graphene hybrid films with high areal capacitance and facile transferability for transparent solid-state supercapacitors. *Energy Storage Mater.* **2020**, *27*, 150–158.
- (26) Yang, B.; Sun, R.; Li, X.; et al. Rapid fabrication of hierarchical porous SiC/C hybrid structure: toward high-performance capacitive energy storage with ultrahigh cyclability. *J. Mater. Sci.* **2021**, *56* (28), 16068–16081.